photonics

Article

Time-Delay Signature Suppression and Communications of Nanolaser Based on Phase Conjugate Feedback

Hao Chen [1], Penghua Mu [1,*], Gang Guo [2], Xintian Liu [2] and Pengfei He [1,*]

[1] School of Physics and Electronic Information, Yantai University, Yantai 264005, China; chenhao2022@s.ytu.edu.cn
[2] FISEC information Technology Company Limited, Weihai 264200, China; gg87@fisherman-it.com (G.G.); liuxintian@fisherman-it.com (X.L.)
* Correspondence: ph_mu@ytu.edu.cn (P.M.); hpf_972@ytu.edu.cn (P.H.)

Abstract: The nonlinear dynamics of nanolasers (NLs), an important component of optical sources, has received much attention. However, there is a lack of in-depth research into the high-quality chaotic output of NLs and their applications in chaotic secure communications. In this paper, we make the NLs generate broadband chaotic signals whose time-delay signatures (TDS) are completely hidden by a phase conjugate feedback structure. And in the two-channel communication scheme, we make the NLs achieve a combination of a low-latency high degree of synchronization and two-channel transmission technique, which enhances the security of message encryption and decryption. We also investigate the effects of system parameters, Purcell factor F, spontaneous emission coupling factor β, and bias current I on the TDS, as well as the effects of parameter mismatch and injection parameters on chaos synchronization and message recovery. The results show that the phase conjugate feedback-based NLs can achieve the suppression of the TDS within a certain parameter range, and it can achieve high-quality synchronization and enhance the security of chaotic communication under appropriate injection conditions.

Keywords: nanolaser; chaos; time-delay signature; communication

Citation: Chen, H.; Mu, P.; Guo, G.; Liu, X.; He, P. Time-Delay Signature Suppression and Communications of Nanolaser Based on Phase Conjugate Feedback. *Photonics* **2024**, *11*, 91. https://doi.org/10.3390/photonics11010091

Received: 22 December 2023
Revised: 6 January 2024
Accepted: 12 January 2024
Published: 19 January 2024

1. Introduction

Optical chaos has attracted a lot of attention in the last two decades, especially in terms of potential applications in chaotic secure communications [1,2], high-speed physical random numbers [3–5], compressed sensing [6], and chaotic lidar/radar [7,8]. However, the feedback action of the external cavity between the laser and the external reflector generates a chaotic time-delay signature (TDS) [9,10], and when such chaotic signals are used as information carriers, they may be extracted by eavesdroppers in order to obtain the key parameters of the communication system and reconfigure them, which, in turn, jeopardizes the security of the chaotic communication system [11]. We also need to focus on the critical issue of laser chaotic bandwidth, which may affect the transmission capacity in chaotic communication, the distance resolution of chaotic lidar, and the rate of random number generation. However, the large size problem arising from most systems consisting of conventional semiconductor lasers and associated auxiliary components may not be suitable for photonic integrated circuits required for practical applications. Therefore, we need to explore a small and novel approach involving using NLs as chaotic entropy sources to generate high-quality broadband chaotic signals and achieve high-quality synchronization between them [12,13].

Currently, time series with specific time-delay can be extracted using standard statistical measurement analysis techniques, which mainly include autocorrelation function (ACF) [14], permutation entropy (PE) [15], and delay mutual information (DMI) [16]. In recent years, how to suppress TDS has become a popular topic of research, for which many published papers have proposed various schemes [17–27]. For example, introducing multiple feedback loops into the system, exploring complex feedback schemes, and adding multiple injection paths have all been considered. NLs have a very small size and volume, and they are able to operate efficiently at low energy inputs with high quantum efficiency. In addition, NLs have fast modulation response speeds, making them suitable for applications such as high-speed communications and data processing. In order to explore the effects of NLs in the integration of photonic circuits, related scholars have conducted experimental studies of their different structures. such as micro-post [28], nano-pillar [29] and bowtie [30], Fabry–Perot [31], nanowire [32], and nano-patch lasers [33], where continuous wave lasing is observed via optical pumping [34] and electrical pumping [35]. The two parameters of the system, Purcell factor F and spontaneous radiation coupling factor β, have a very great influence on the dynamic characteristics of the NLs. K.A. Shore et al.'s studies analyzed the dynamic behavior of the NL under current modulation [36], optical feedback [37], optical injection [38], and inter-injection [39], respectively, and described in detail the effects of the relevant parameters, such as the Purcell factor F, and the effects of relevant parameters, such as spontaneous radiation coupling factor β, on the laser output are elaborated in detail. In addition, Han et al. further investigated the dynamics of mutually coupled semiconductor NLs and observed a rich dynamic output [40–43]. Elsonbaty et al. investigated the TDS of a single NL using a hybrid all-optical and electro-optical feedback scheme and compared the chaotic characteristics generated under normal optical feedback, phase conjugate optical feedback, and grating-mirror optical feedback [44]. Xiang [45] et al. demonstrated that chaotic signals with completely hidden TDS can be output from NLs in a dual chaotic injection system over a wide range of parameters. Based on the above studies, we can show that the laser properties are different to those of conventional mirror feedback. It is due to the property of a phase conjugate mirror, which reverses the phase of the reflected light with respect to the incident light, resulting in zero external cavity round trip phase change. From this, it can be predicted that NLs can be well implemented for TDS hiding by means of phase conjugate feedback, and we further investigate the synchronization characteristics and communication security under the corresponding structure.

The aim of this paper is that the master nanolaser (MNL) is fed back by the phase conjugate mirror and then further injected into the two slave nanolasers (SNL_1 and SNL_2) in parallel. In the simulation, we will quantify the TDS of the signals by introducing the autocorrelation function (ACF) and systematically analyze the dynamics of the MNL and the TDS of the output signals of the system under different feedback parameters. At the same time, we will study the effect of internal parameter mismatch and the differences between injection parameters on chaotic synchronization and communication for SNL_1 and SNL_2 [46]. The paper is organized as follows: Section 2 describes the delay suppression and synchronous communication model of an NL through phase conjugate feedback and parallel injection of SNL_1 and SNL_2, as well as the corresponding rate equations and parameter definitions. Section 3 presents the simulation results related to the above study. Finally, Section 4 provides the basic conclusions based on the simulation results.

2. Theoretical Model

The structure of the NL chaotic system is shown in Figure 1, including the master nanolaser (MNL) and two slave nanolasers (SNL_1 and SNL_2). The MNL is fed back by a phase conjugate mirror, and under appropriate feedback conditions, the MNL exhibits chaotic oscillation phenomena and generates rich nonlinear dynamics, as shown in Figure 1. The feedback intensity of the MNL and the injection intensity of the MNL into SNL_1 and SNL_2 are regulated by variable attenuators (VA_1, VA_2, and VA_3), and the optical isolators (OI_1 and OI_2) ensure that the MNL can be unidirectionally injected into SNL_1 and SNL_2, respectively. The control parameters in this system include the feedback parameter, injection parameter, bias currents I, Purcell factor F, and spontaneous emission coupling factor β. The L-K rate equation of the NL system studied in this paper is modeled as shown in [38].

$$\begin{aligned}\frac{dI_M(t)}{dt} &= \Gamma\left[\frac{F\beta N_M(t)}{\tau_n} + \frac{g_n(N_M(t)-N_0)}{1+\varepsilon I_M(t)} I_M(t)\right] - \frac{1}{\tau_p} I_M(t) \\ &+2k_d\sqrt{I_M(t)I_M(t-\tau_d)}\cos(\theta_1(t)) + F_I(t)\end{aligned} \tag{1}$$

$$\frac{d\phi_M(t)}{dt} = \frac{\alpha}{2}\Gamma g_n(N_M(t)-N_{th}) - k_d\frac{\sqrt{I_M(t-\tau_d)}}{\sqrt{I_M(t)}}\sin(\theta_1(t)) + F_\phi(t) \tag{2}$$

$$\frac{dN_M(t)}{dt} = \frac{I_{dc}}{eV_a} - \frac{N_M(t)}{\tau_n}(F\beta+1-\beta) - \frac{g_n(N_M(t)-N_0)}{1+\varepsilon I_M(t)} I_M(t) + F_N(t) \tag{3}$$

$$\begin{aligned}\frac{dI_{S1|S2}(t)}{dt} &= \Gamma\left[\frac{F\beta N_{S1|S2}(t)}{\tau_n} + \frac{g_n\left(N_{S1|S2}(t)-N_0\right)}{1+\varepsilon I_{S1|S2}(t)} I_{S1|S2}(t)\right] - \frac{1}{\tau_p} I_{S1|S2}(t) \\ &+2k_{ri}\sqrt{I_{S1|S2}(t)I_{M|M}(t-\tau_{ri})}\cos\left(\theta_j(t)\right)\end{aligned} \tag{4}$$

$$\frac{d\phi_{S1|S2}(t)}{dt} = \frac{\alpha}{2}\Gamma g_n\left(N_{I|S}(t)-N_{th}\right) - 2\pi\Delta f_i - k_{ri}\frac{\sqrt{I_{M|M}(t-\tau_{ri})}}{\sqrt{I_{S1|S2}(t)}}\sin\left(\theta_j(t)\right) \tag{5}$$

$$\frac{dN_{S1|S2}(t)}{dt} = \frac{I_{dc}}{eV_a} - \frac{N_{S1|S2}(t)}{\tau_n}(F\beta+1-\beta) - \frac{g_n\left(N_{S1|S2}(t)-N_0\right)}{1+\varepsilon I_{S1|S2}(t)} I_{S1|S2}(t) \tag{6}$$

$$\theta_1(t) = \phi_M(t) - \phi_M(t-\tau_d) \tag{7}$$

$$\theta_j(t) = 2\pi f_{M|M}\tau_{ri} + \phi_{S1|S2}(t) - \phi_{M|M}(t-\tau_{ri}) - 2\pi\Delta f_i t (i=1,2; j=2,3) \tag{8}$$

$$F_I(t) = \sqrt{\frac{2I(t)\beta N(t)}{\tau_n\Delta t}}\mathrm{x}_I \tag{9}$$

$$F_n(t) = -\sqrt{\frac{2I(t)\beta N(t)}{\tau_n\Delta t}}\mathrm{x}_s + \sqrt{\frac{2N(t)}{\tau_n\Delta t V_a}}\mathrm{x}_n \tag{10}$$

$$F_\phi(t) = \frac{1}{I(t)}\sqrt{\frac{2I(t)\beta N(t)}{2\tau_n\Delta t}}\mathrm{x}_\phi \tag{11}$$

In the above rate equations, the subscripts 'M', 'S1', and 'S2' denote MNL, SNL_1, and SNL_2, respectively. $I(t)$ is the photon density, $\phi(t)$ is the phase, and $N(t)$ is the carrier density. F is the Purcell factor, β is the spontaneous radiation coupling factor, Γ is the confinement factor, and τ_n and τ_p are the carrier lifetime and the photon lifetime. g_n is the differential gain, N_0 is the transparency carrier density, ε is the gain saturation factor, and α is the linewidth enhancement factor. $I_{dc} = qI_{th}$ is the laser operating current, I_{th} is the threshold current with respect to F and β, V_a is the volume of the active region, e is the electron charge, and N_{th} is the threshold carrier density.

In the optical feedback parts of Equations (1) and (2), the feedback strength of the feedback path k_d and the feedback delay τ_d are included. k_d can be expressed as follows [38]

$$k_d = f(1-R)\sqrt{\frac{R_{ext}}{R}}\frac{c}{2nL} \tag{12}$$

where f is the feedback coupling factor, which can be adjusted in the model to determine the feedback strength k_d; c is the speed of light in free space; n is the refractive index; and L is the feedback cavity length. R is the reflectivity of the NL and R_{ext} is the specular reflectivity. Optical injection into both from the NL is controlled by the injection rate k_{ri}, while k_{ri} and τ_{ri} are the injection rate and injection delay, respectively. R_{inj} is the injection coefficient, and k_{ri} can be expressed as follows [38]:

$$k_{ri} = (1-R)\sqrt{\frac{R_{inj}}{R}}\frac{c}{2nL} \tag{13}$$

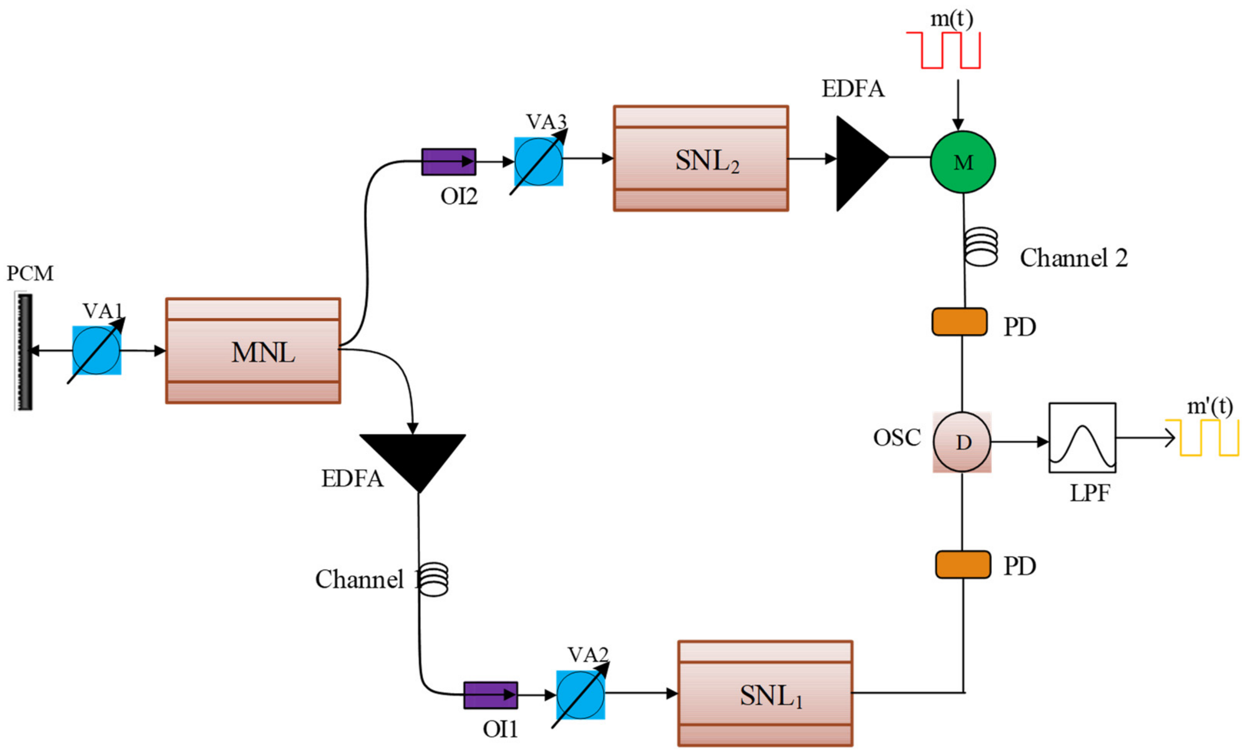

Figure 1. Architecture for phase conjugate feedback-based time-delay signal suppression and communication in nanolasers. MNL: master nanolaser; SNL_1: slave nanolaser 1; SNL_2: slave nanolaser 2; PCM: phase conjugate feedback mirror; VA: variable attenuator; OI: optical isolator; LPF: low-pass filter; EDFA: erbium-doped optical fiber amplifier; m: modulator; PD: photodiode; m(t): message; m′(t): decrypted message.

In Equations (9)–(11), the symbols x_I, x_n, and x_ϕ are Gaussian distributed random variables with zero mean and unit variance. The rate equations with phase conjugate feedback and Langevin noise terms are solved numerically using the Runge–Kutta algorithm. The Langevin noise is modeled by applying the random noise as computed, where the noise interval Δt is 0.5 ps. Table 1 lists some of the important parameters used in the simulation of the NL system and the corresponding parameter annotations.

In order to quantify the TDS of the signal, we used the autocorrelation function (ACF), and in the following study, the TDS is considered to be hidden when the peak value of the ACF is less than 0.2. The ACF is defined as follows [43,44]:

$$C(\Delta t) = \frac{\langle [I(t+\Delta t) - \langle I(t+\Delta t)\rangle][I(t) - \langle I(t)\rangle]\rangle}{\sqrt{\left\langle [I(t+\Delta t) - \langle I(t+\Delta t)\rangle]^2 \right\rangle \left\langle [I(t) - \langle I(t)\rangle]^2 \right\rangle}} \tag{14}$$

where <> denotes the average value of the time series $I(t)$, Δt denotes the time shift, ACF denotes a comparison between the similarity of a signal and itself at different points in time, when the lower the autocorrelation value, the higher the unpredictability of the chaotic stochastic sequences, as well as the more difficult it is to be extracted into useful information.

Table 1. Parameters used in the numerical simulations [38].

Parameter	Description	Value
Γ	Confinement factor	0.645
τ_n	Carrier lifetime	1 ns
τ_p	Photon lifetime	0.36 ps
td	Feedback delay	0.2 ns
g_n	Differential gain	1.65×10^{-6} cm^3/s
N_0	Transparency carrier density	1.1×10^{-18} cm^{-3}
ε	Gain saturation factor	2.3×10^{-17} cm^3
α	Linewidth enhancement factor	5
V_a	Volume of active region	3.96×10^{-13} cm^3
λ	Wavelength of NL	1591 nm
R	Laser facet reflectivity	0.85
R_{ext}	External facet power reflectivity	0.95
R_{inj}	Injection ratio	0–0.1
n	Refractive index	3.4
L	Cavity length	1.39 μm
Q	Quality factor	428
f	Feedback coupling fraction	0–0.9

3. Simulation Results

In this section, we simulate the laser rate equations of the system using the fourth-order Runge–Kutta algorithm. Firstly, the nonlinear dynamics of the MNL is investigated, and suitable parameters are chosen so that the two parallel injected SNLs operate in a chaotic state. Then, the focus is on the synchronization performance of the two SNLs under equal and unequal frequency detuning as the injection intensity varies. Through these studies, we identify the range of parameters that enable the SNLs to be highly synchronized and further apply them to relevant chaotic secure communications.

The output of the NL can be controlled by varying the feedback parameter to control the nonlinear dynamical system. Figure 2a,b show the intensity time series and ACF plots of the MNL at a feedback parameter of 0.02, while (c) and (d) represent the intensity time series and ACF plots of the MNL at a feedback parameter of 0.2. Here, the relevant parameters are set as F = 14, β = 0.05, $I = 2I_{th}$, and I_{th} = 1.127 mA. It can be seen from the Figure 2 that the MNL works in chaotic state when the feedback parameters are 0.02 and 0.2. At the same time, their corresponding ACF values at the time-delay of 0.2 ns are both less than 0.2, indicating that the TDS of the output chaotic signal is completely hidden. Then, the ACF line graphs of the MNL are investigated according to the variation in the feedback parameters under F = 14, β = 0.05, F = 14, β = 0.1, and F = 30, β = 0.1, respectively. From Figure 3, it can be observed that as the feedback parameters increase, the ACF value of the MNL gradually increases in all three different cases, but the corresponding ACF values in this interval range are less than 0.2. This indicates that the delay of the MNL can be well suppressed and is conducive to the subsequent study of the synchronous communication of the two SNLs. When F = 30 and β = 0.1, the ACF of MNL greatly increases with the increase in the feedback parameters because the larger the values of F and β, the greater the damping of the relaxation oscillation of NL [47]. Therefore, we can use medium F and small β to better hide the TDS of NLs in a wider parameter space.

In practice, parameter mismatch is inevitable. We proceed to study the synchronization performance in the presence of mismatched parameters between the two SNLs.

There are two different cases: Case 1 is that MNL is equal to the frequency detuning between SNL_1 and SNL_2, and Case 2 is that MNL is unequal to the frequency detuning between SNL_1 and SNL_2.

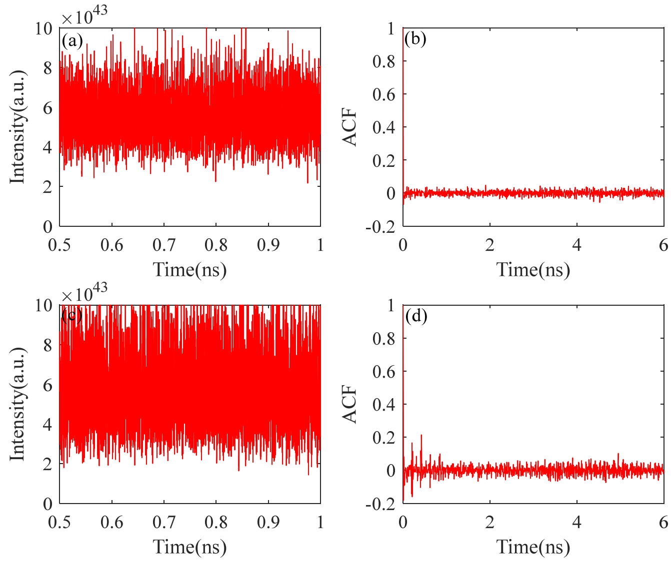

Figure 2. (**a**,**b**) The intensity time series and (**c**,**d**) computed ACF of MNL for two feedback coupling ratios: (**a**,**c**) f = 0.02 and (**b**,**d**) f = 0.2.

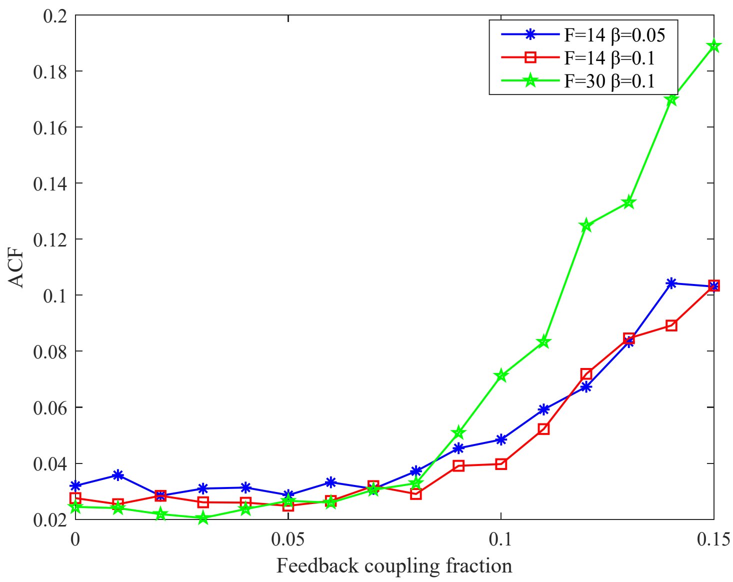

Figure 3. MNL with feedback parameters at F = 14, β = 0.05, F = 14, β = 0.1, F = 30, and β = 0.1.

3.1. *Case 1: MNL Is Equal to the Frequency Detuning between SNL_1 and SNL_2*

We investigate the correlation coefficient C_{TR} of the two SNLs with respect to the variation in the injected intensity k_{inj1} and k_{inj2} when the MNL is equal to the frequency detuning of the two SNLs. In the simulation, we choose different parameter values as $\Delta f_1 = \Delta f_2 = 10$ GHz, $\Delta f_1 = \Delta f_2 = 15$ GHz, and $\Delta f_1 = \Delta f_2 = -15$ GHz. It can be seen in Figure 4a that when the frequency detuning $\Delta f_1 = \Delta f_2 = 10$ GHz, the region of highly synchronous SNL_1 and SNL_2 is almost in the range of a 45° angle and will be larger and larger with the increase in the injection intensity. When the frequency detuning is increased to 15 GHz in Figure 4b, it is clearly observed that a higher injection strength is required to enable the two SNLs to be highly synchronized. In Figure 4c, when the frequency detuning is −15 GHz, it can be clearly observed that the range of achieving high synchronization between the two SNLs is much wider, and a wider region can be achieved with good synchronization at a very small range of injection strength.

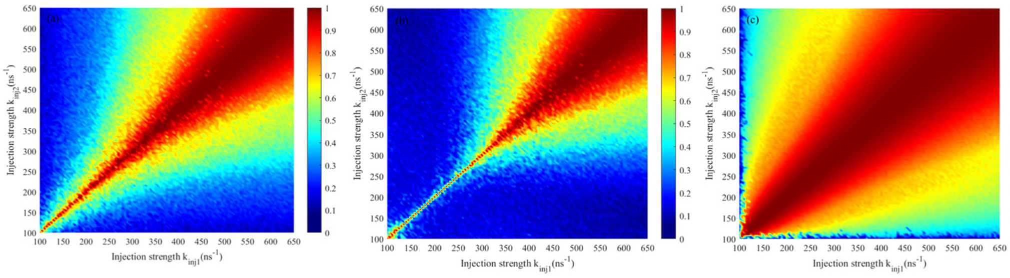

Figure 4. Correlation coefficients C_{TR} of SNL_1 and SNL_2 for frequency detuning Δf_1 and Δf_2: (**a**) $\Delta f_1 = \Delta f_2 = 10$ GHz; (**b**) $\Delta f_1 = \Delta f_2 = 15$ GHz; (**c**) $\Delta f_1 = \Delta f_2 = -15$ GHz.

3.2. Case 2: MNL Is Unequal to the Frequency Detuning between SNL_1 and SNL_2

Then, we investigated the case when the MNL is not equal to the frequency detuning of the two SNLs. In Figure 5a, when the frequency detuning $\Delta f_1 = 10$ GHz, $\Delta f_2 = 15$ GHz, the synchronization effect of the two SNLs is obviously weakened, and a larger injection intensity is required to achieve a highly synchronized effect. In Figure 5b,c, when the frequency detuning is $\Delta f_1 = -15$ GHz, $\Delta f_2 = 10$ GHz and $\Delta f_1 = -15$ GHz, and $\Delta f_2 = 15$ GHz, respectively, the synchronization effect achieved is similar to that of Figure 5a. At high injection intensity, the two SNLS will be locked via MNL injection so that the synchronization effect between them is less affected by the change in the injection rate. Finally, in Figure 5d, when the frequency detuning $\Delta f_1 = -15$ GHz and $\Delta f_2 = -5$ GHz, it can be seen that when the frequency detuning is negative, the synchronization performance of the two SNLs is better than that shown in the above figure. This is because when the frequency detuning of the two SNLs is negative, their resonant frequencies will be closer to each other, which is more helpful for promoting synchronization between them.

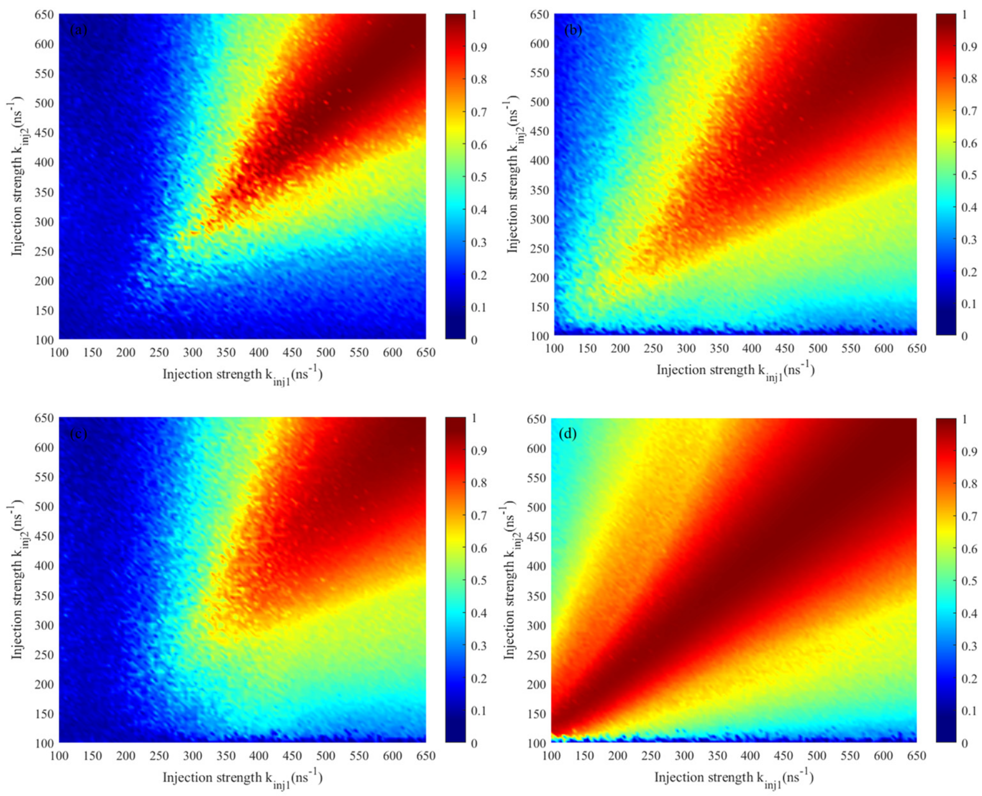

Figure 5. Correlation coefficients C_{TR} of SNL_1 and SNL_2 under frequency detuning Δf_1 and Δf_2: (**a**) $\Delta f_1 = 10$ GHz, $\Delta f_2 = 15$ GHz; (**b**) $\Delta f_1 = -5$ GHz, $\Delta f_2 = 10$ GHz; (**c**) $\Delta f_1 = -15$ GHz, $\Delta f_2 = 15$ GHz; (**d**) $\Delta f_1 = -15$ GHz, $\Delta f_2 = -5$ GHz.

Subsequently, we investigate the ACF of SNL_1 at frequency detuning of -15 GHz, 10 GHz, and 15 GHz, respectively. From Figure 6, it can be found that the TDS of SNL_1 are all well suppressed at an injection strength of 300 ns^{-1}. This is mainly due to the fact that the high injection rate causes SNL_1 to be locked by the MNL injection, and, thus, the TDS of MNL are shown to be well hidden. The TDS of SNL_2 is similar to those of SNL_1 due to the injection strength k_{inj1} = k_{inj2} in the subsequent study.

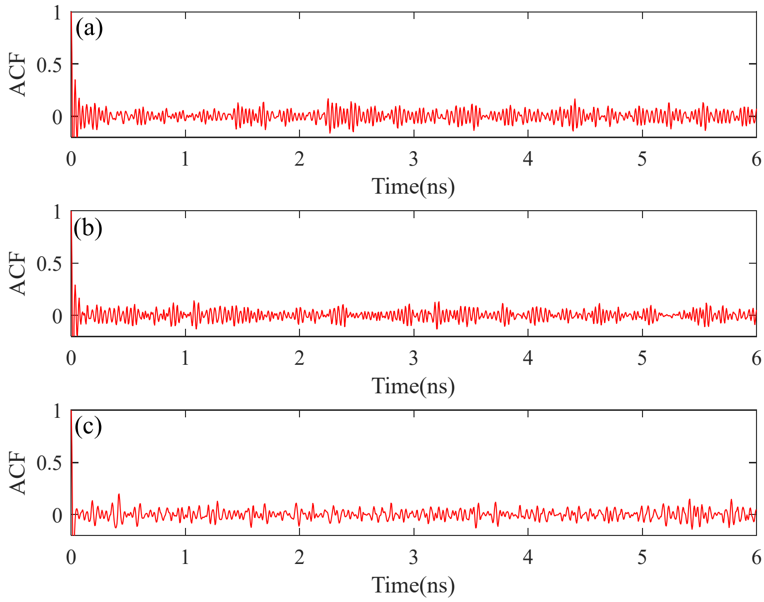

Figure 6. ACF of SNL_1 at frequency detuning of Δf_1: (**a**) Δf_1 = -15 GHz; (**b**) Δf_1 = 10 GHz; (**c**) Δf_1 = 15 GHz.

To further investigate the effect of internal parameter mismatch on the synchronization of the two SNLs, we fixed the parameters of SNL_1 and varied the parameters of SNL_2 according to the associated mismatch ratio u, where $u = \frac{\Pi^{SNL_1} - \Pi^{SNL_2}}{\Pi^{SNL_1}}$. We also fixed the external parameters, such as injection strength and frequency detuning, to be the same for both SNLs. The variation in the associated peak C_{TR} with the mismatch ratio u when k_{inj1} = k_{inj2} = 300 ns^{-1} is shown in Figure 7a. It can be observed from the figure that the synchronization performance corresponding to the five mismatched parameters is also different at moderate injection intensity. As the parameter mismatch ratio increases, the corresponding correlation peak C_{TR} decreases, but the overall value of C_{TR} is greater than 0.95, indicating that the system can still achieve high-quality chaotic synchronization. When the injection rate is very large, i.e., k_{inj1} = k_{inj2} = 600 ns^{-1}, it can be seen from Figure 7b that the variation in the parameter mismatch u has less effect on the chaotic synchronization. Therefore, the difference in the synchronization and decoding characteristics of the system when the parameters are mismatched is not significant, which also indicates that that the system is robust to parameter mismatch.

Before the message encoding and decoding process, we fixed the frequency detuning of both SNLs to -15 GHz and investigated the corresponding transmission bandwidths. Figure 8 shows the spectrograms of the chaotic carriers generated by the SNL_1 by varying F and β at injection currents of $I = 2$Ith and $I = 4$Ith, respectively. We define the effective bandwidth as the range between DC and the frequency containing 80% of the spectral power. When the injection current is set at $I = 2$Ith, the effective bandwidths are 36.6 GHz, 22.8 GHz, and 13.3 GHz for (F, β) values of (14, 0.05), (14, 0.1), and (30, 0.1). In comparison, the effective bandwidths for the same (F, β) settings are 35.8 GHz, 21.8 GHz, and 11.8 GHz when the injection current is set at $I = 4$Ith. These results show that the system is capable of achieving broadband chaos and, hence, high-speed message transmission when all factors are considered. However, we also need to ensure that the TDS can be completely hidden to ensure the security of the communication and prevent information leakage. By choosing the appropriate F, β, and injection current, i.e., F = 14, β = 0.05, and I = 2Ith, the system can be made to stably output chaotic signals with time-delay hiding, bandwidth enhancement, and a high degree of unpredictability.

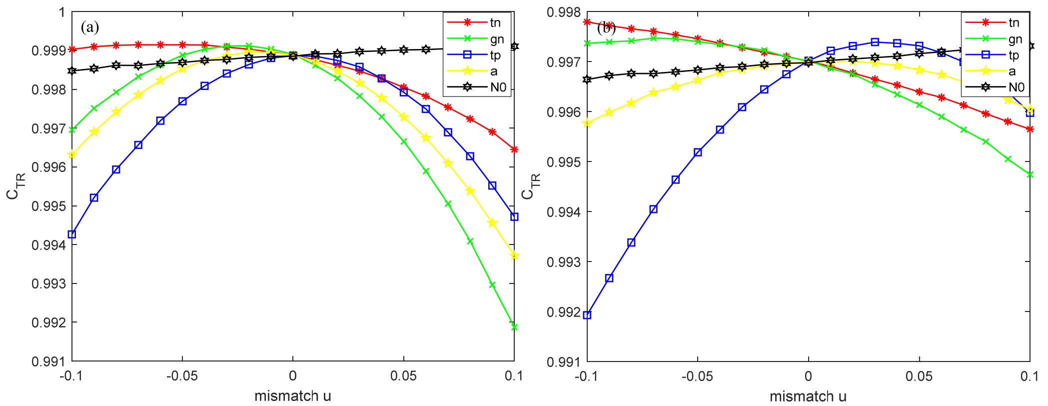

Figure 7. Correlation peak as a function of the relative mismatch ratio for (1) τ_n, (2) g_n, (3) τ_p, (4) α, and (5) N_0. (**a**) k_{inj1} = k_{inj2} = 300 ns^{-1}, (**b**) k_{inj1} = k_{inj2} = 600 ns^{-1}. Δf_1 = Δf_2 = −15 GHz.

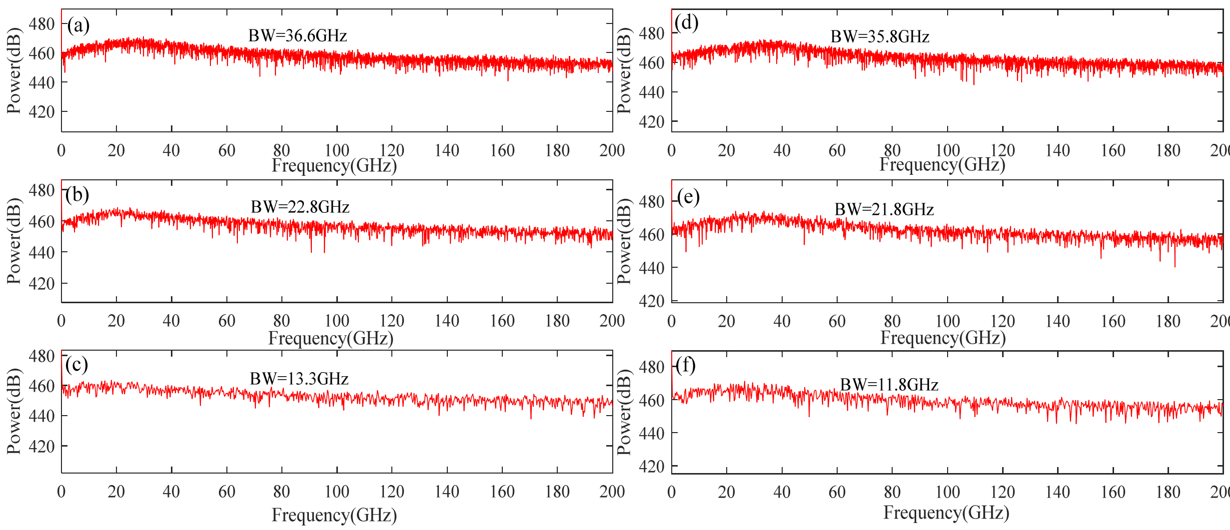

Figure 8. Power spectra for SNL_1 under different values of F, β, and injection current: (**a**–**c**) I = 2Ith and (**d**–**f**) I = 4Ith; (**a**,**d**) F = 14 and β = 0.05; (**b**,**e**) F = 14 and β = 0.1; (**c**,**f**) F = 30 and β = 0.1.

Finally, we conducted a related study of the encoding and decoding process of the messages. Based on the above studies, the frequency detuning and injection rate parameters were fixed at −15 GHz and 300 ns^{-1}, enabling the two SNLs to have low latency, high bandwidth, and high synchronization performance. The CMO encryption method is used in Figure 9, where a small-amplitude message is used to modulate the laser signal output. The mathematical expression is $I_{ext}(t) = I(t)[1 + h_{CMO}m(t)]$, where h_{CMO} denotes the modulation depth and $m(t)$ denotes the message to be transmitted. In a two-channel communication system, the drive signal from the MNL is transmitted through channel 1 for high-quality chaotic synchronization between SNL_1 and SNL_2, while the modulation signal $I_{ext}(t)$ is transmitted through channel 2. Therefore, at the SNL_1 end, we can obtain the differential signal by subtracting the output of SNL_1 from the transmitted signal and then filter the differential signal using a fifth-order Butterworth filter with a cutoff frequency equal to 0.6 × B_S to obtain the recovered message (where B_S is the bit rate of the message, and B_S = 8 Gbit/s is taken as an example in this study).

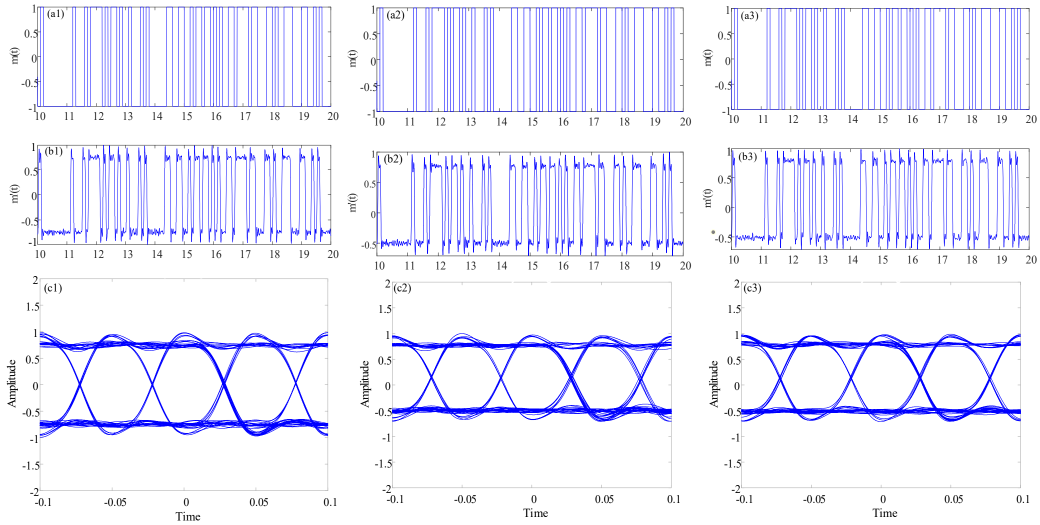

Figure 9. Coding and decoding process of SNL_1 and SNL_2 at a modulation depth of h_{CMO} = 0.6. (**a1**–**a3**) The original message at 8 Gbit/s, (**b1**–**b3**) the recovered message, and (**c1**–**c3**) the eye diagram. (**a1**–**c1**) kr2 = kr3 = 300 ns^{-1} and no mismatch, (**a2**–**c2**) kr2 = kr3 = 300 ns^{-1} and mismatch of u = 0.1, and (**a3**–**c3**) kr2 = kr3 = 600 ns^{-1} and mismatch of u = 0.1.

Figure 9 shows the results of the message encryption and decryption process. Firstly, we illustrate the quality of the recovered messages without considering parameter mismatches, using the quality factor $Q = (I_1 - I_0)/(\sigma_1 + \sigma_0)$ and the eye diagram, where I_1 and I_0 are the average optical power values of bits "1" and "0". σ_1 and σ_0 are the corresponding standard deviations. We stipulate that the quality factor Q > 6 is sufficient for communication, i.e., BER < 10^{-9}. The original message $m(t)$, the recovered message $m\prime(t)$, and the corresponding eye diagrams are depicted for a h_{CMO} = 0.6 modulation depth. From Figure 9(a1–c1), it can be seen that the message can be fully recovered at a moderate injection rate without parameter mismatch, corresponding to Q = 10.41, and the eye diagram is clear and widely open. Then, parameter mismatches are introduced for SNL_2: ${\tau_n}^{SNL_2} = (1+u){\tau_n}^{SNL_1}$, ${g_n}^{SNL_2} = (1-u){g_n}^{SNL_1}$, ${\tau_p}^{SNL_2} = (1-u){\tau_p}^{SNL_1}$, ${\alpha_n}^{SNL_2} = (1-u){\alpha_n}^{SNL_1}$, and ${N_0}^{SNL_2} = (1+u){N_0}^{SNL_1}$. This is shown in Figure 9(a2–c2), where the mismatch ratio u = 0.1 is set and the injection rate is constant. We can clearly see that the value of the quality factor Q of SNL_2 decreases to 9.99, but it still satisfies the requirement that Q is greater than 6, and, thus, the eye diagram is still able to demonstrate openness, i.e., it is better able to recover the same message. This corroborates with the effect of parameter mismatch on synchronization performance described above and proves that the system is robust to parameter mismatch. Finally, keeping the mismatch ratio u = 0.1 and increasing the injection rate to a reasonable 600 ns^{-1} is used to compensate for the degradation due to mismatch. The corresponding results are shown in Figure 9(a3–c3), where the value of quality factor Q is 10.24, which further improves the message recovery. However, the security of the system may be affected when the injection rate is too large, so we should choose appropriate injection parameters to enable the system to achieve a high synchronization performance and enhance the security of chaotic communication.

4. Conclusions

In summary, the NL is capable of generating high-quality chaotic signals with low time-delay, wide bandwidth, and high synchronization signature through phase conjugate feedback and then parallel injection into SNL_1 and SNL_2. The effects of system parameters, Purcell factor F, spontaneous radiation coupling factor β, and bias current I on the TDS hiding and bandwidth of chaotic output from the NL are investigated in detail. Then, we applied the output chaotic signals to two-channel communication and further investigated the effects of injection parameters, as well as internal parameter mismatch, on chaotic synchronous communication. According to this study, the selection of appropriate injection parameters can make the NL stably output chaotic signals with time-delay hiding, bandwidth enhancement, and high unpredictability, as well as enhance the security of chaotic communication. The research presented in this paper offers important theoretical guidance for the practical application of NL chaotic systems.

Author Contributions: Methodology, H.C. and P.M.; validation, G.G. and P.M.; investigation, X.L. and P.H.; writing—original draft preparation, H.C. and G.G.; writing—review and editing, H.C., X.L., P.M. and G.G. All authors have read and agreed to the published version of the manuscript.

Funding: This work was supported by the Project: Natural Science Foundation of Shandong Provincial (ZR2020QF090), the Key Laboratory of Modern Optical Technologies of Education Ministry of China, Soochow University (KJS2066); and the Key Laboratory of Advanced Optical Manufacturing Technologies of Jiangsu Province, Soochow University (KJS2045).

Institutional Review Board Statement: Not applicable.

Informed Consent Statement: Not applicable.

Data Availability Statement: Data are contained within the article.

Acknowledgments: The authors would like to thank all the reviewers for their helpful comments and suggestions on this paper.

Conflicts of Interest: The authors declare no conflict of interest.

References

1. Argyris, A.; Syvridis, D.; Larger, L.; Annovazzi-Lodi, V.; Colet, P.; Fischer, I.; García-Ojalvo, J.; Mirasso, C.R.; Pesquera, L.; Shore, K.A. Chaos-Based Communications at High Bit Rates Using Commercial Fibre-Optic Links. *Nature* **2005**, *438*, 343–346. [CrossRef] [PubMed]
2. Terry, J.R.; VanWiggeren, G.D. Chaotic Communication Using Generalized Synchronization. *Chaos Solitons Fractals* **2001**, *12*, 145–152. [CrossRef]
3. Uchida, A.; Amano, K.; Inoue, M.; Hirano, K.; Naito, S.; Someya, H.; Oowada, I.; Kurashige, T.; Shiki, M.; Yoshimori, S.; et al. Fast Physical Random Bit Generation with Chaotic Semiconductor Lasers. *Nat. Photonics* **2008**, *2*, 728–732. [CrossRef]
4. Li, N.; Kim, B.; Chizhevsky, V.N.; Locquet, A.; Bloch, M.; Citrin, D.S.; Pan, W. Two Approaches for Ultrafast Random Bit Generation Based on the Chaotic Dynamics of a Semiconductor Laser. *Opt. Express* **2014**, *22*, 6634. [CrossRef] [PubMed]
5. Li, X.-Z.; Chan, S.-C. Random Bit Generation Using an Optically Injected Semiconductor Laser in Chaos with Oversampling. *Opt. Lett.* **2012**, *37*, 2163. [CrossRef]
6. Rontani, D.; Choi, D.; Chang, C.-Y.; Locquet, A.; Citrin, D.S. Compressive Sensing with Optical Chaos. *Sci. Rep.* **2016**, *6*, 35206. [CrossRef] [PubMed]
7. Lin, F.-Y.; Liu, J.-M. Chaotic Lidar. *IEEE J. Sel. Top. Quantum Electron.* **2004**, *10*, 991–997. [CrossRef]
8. Lin, F.-Y.; Liu, J.-M. Chaotic Radar Using Nonlinear Laser Dynamics. *IEEE J. Quantum Electron.* **2004**, *40*, 815–820. [CrossRef]
9. Wu, J.-G.; Xia, G.-Q.; Tang, X.; Lin, X.-D.; Deng, T.; Fan, L.; Wu, Z.-M. Time Delay Signature Concealment of Optical Feedback Induced Chaos in an External Cavity Semiconductor Laser. *Opt. Express* **2010**, *18*, 6661. [CrossRef]
10. Udaltsov, V.S.; Goedgebuer, J.-P.; Larger, L.; Cuenot, J.-B.; Levy, P.; Rhodes, W.T. Cracking Chaos-Based Encryption Systems Ruled by Nonlinear Time Delay Differential Equations. *Phys. Lett. A* **2003**, *308*, 54–60. [CrossRef]
11. Zhao, Q.; Wang, Y.; Wang, A. Eavesdropping in Chaotic Optical Communication Using the Feedback Length of an External-Cavity Laser as a Key. *Appl. Opt.* **2009**, *48*, 3515. [CrossRef] [PubMed]
12. Madani, A.; Ma, L.; Miao, S.; Jorgensen, M.R.; Schmidt, O.G. Luminescent Nanoparticles Embedded in TiO_2 Microtube Cavities for the Activation of Whispering-Gallery-Modes Extending from the Visible to the near Infrared. *Nanoscale* **2016**, *8*, 9498–9503. [CrossRef] [PubMed]
13. Madani, A.; Bolaños Quiñones, V.A.; Ma, L.B.; Miao, S.D.; Jorgensen, M.R.; Schmidt, O.G. Overlapping Double Potential Wells in a Single Optical Microtube Cavity with Vernier-Scale-like Tuning Effect. *Appl. Phys. Lett.* **2016**, *108*, 171105. [CrossRef]
14. Rontani, D.; Locquet, A.; Sciamanna, M.; Citrin, D.S. Loss of Time-Delay Signature in the Chaotic Output of a Semiconductor Laser with Optical Feedback. *Opt. Lett.* **2007**, *32*, 2960. [CrossRef]
15. Soriano, M.C.; Zunino, L.; Rosso, O.A.; Fischer, I.; Mirasso, C.R. Time Scales of a Chaotic Semiconductor Laser With Optical Feedback Under the Lens of a Permutation Information Analysis. *IEEE J. Quantum Electron.* **2011**, *47*, 252–261. [CrossRef]
16. Rontani, D.; Locquet, A.; Sciamanna, M.; Citrin, D.S.; Ortin, S. Time-Delay Identification in a Chaotic Semiconductor Laser With Optical Feedback: A Dynamical Point of View. *IEEE J. Quantum Electron.* **2009**, *45*, 879–1891. [CrossRef]

17. Wu, J.-G.; Xia, G.-Q.; Wu, Z.-M. Suppression of Time Delay Signatures of Chaotic Output in a Semiconductor Laser with Double Optical Feedback. *Opt. Express* **2009**, *17*, 20124. [CrossRef]
18. Zhong, Z.-Q.; Wu, Z.-M.; Xia, G.-Q. Experimental Investigation on the Time-Delay Signature of Chaotic Output from a 1550 Nm VCSEL Subject to FBG Feedback. *Photonics Res.* **2017**, *5*, 6. [CrossRef]
19. Priyadarshi, S.; Hong, Y.; Pierce, I.; Shore, K.K. Experimental Investigations of Time-Delay Signature Concealment in Chaotic External Cavity VCSELs Subject to Variable Optical Polarization Angle of Feedback. *IEEE J. Sel. Top. Quantum Electron.* **2013**, *19*, 1700707. [CrossRef]
20. Li, N.; Pan, W.; Locquet, A.; Citrin, D.S. Time-Delay Concealment and Complexity Enhancement of an External-Cavity Laser through Optical Injection. *Opt. Lett.* **2015**, *40*, 4416. [CrossRef]
21. Li, N.; Pan, W.; Xiang, S.; Yan, L.; Luo, B.; Zou, X.; Zhang, L.; Mu, P. Photonic Generation of Wideband Time-Delay-Signature-Eliminated Chaotic Signals Utilizing an Optically Injected Semiconductor Laser. *IEEE J. Quantum Electron.* **2012**, *48*, 1339–1345. [CrossRef]
22. Hong, Y. Experimental Study of Time-Delay Signature of Chaos in Mutually Coupled Vertical-Cavity Surface-Emitting Lasers Subject to Polarization Optical Injection. *Opt. Express* **2013**, *21*, 17894. [CrossRef] [PubMed]
23. Wu, J.-G.; Wu, Z.-M.; Xia, G.-Q.; Feng, G.-Y. Evolution of Time Delay Signature of Chaos Generated in a Mutually Delay-Coupled Semiconductor Lasers System. *Opt. Express* **2012**, *20*, 1741. [CrossRef]
24. Mu, P.; Pan, W.; Yan, L.; Luo, B.; Li, N.; Xu, M. Experimental Evidence of Time-Delay Concealment in a DFB Laser With Dual-Chaotic Optical Injections. *IEEE Photonics Technol. Lett.* **2016**, *28*, 131–134. [CrossRef]
25. Hong, Y.; Quirce, A.; Wang, B.; Ji, S.; Panajotov, K.; Spencer, P.S. Concealment of Chaos Time-Delay Signature in Three-Cascaded Vertical-Cavity Surface-Emitting Lasers. *IEEE J. Quantum Electron.* **2016**, *52*, 2400508. [CrossRef]
26. Li, N.; Pan, W.; Xiang, S.; Yan, L.; Luo, B.; Zou, X. Loss of Time Delay Signature in Broadband Cascade-Coupled Semiconductor Lasers. *IEEE Photonics Technol. Lett.* **2012**, *24*, 2187–2190. [CrossRef]
27. Zeng, Y.; Wang, Y.; Gu, S.; Huang, Y.; Zhou, P.; Mu, P.; Li, N. Chaotic Characteristics Enhancement by Introducing Optical Feedback into a Sole Intensity Modulation Optical Injection System. *J. Opt. Soc. Am. B* **2023**, *40*, 1726. [CrossRef]
28. Pelton, M.; Santori, C.; Vučković, J.; Zhang, B.; Solomon, G.S.; Plant, J.; Yamamoto, Y. Efficient Source of Single Photons: A Single Quantum Dot in a Micropost Microcavity. *Phys. Rev. Lett.* **2002**, *89*, 233602. [CrossRef]
29. Reitzenstein, S.; Heindel, T.; Kistner, C.; Rahimi-Iman, A.; Schneider, C.; Höfling, S.; Forchel, A. Low Threshold Electrically Pumped Quantum Dot-Micropillar Lasers. *Appl. Phys. Lett.* **2008**, *93*, 061104. [CrossRef]
30. Chang, S.-W.; Ni, C.-Y.A.; Chuang, S.-L. Theory for Bowtie Plasmonic Nanolasers. *Opt. Express* **2008**, *16*, 10580. [CrossRef]
31. Hill, M.T.; Marell, M.; Leong, E.S.P.; Smalbrugge, B.; Zhu, Y.; Sun, M.; Van Veldhoven, P.J.; Geluk, E.J.; Karouta, F.; Oei, Y.-S.; et al. Lasing in Metal-Insulator-Metal Sub-Wavelength Plasmonic Waveguides. *Opt. Express* **2009**, *17*, 11107. [CrossRef]
32. Oulton, R.F.; Sorger, V.J.; Zentgraf, T.; Ma, R.-M.; Gladden, C.; Dai, L.; Bartal, G.; Zhang, X. Plasmon Lasers at Deep Subwavelength Scale. *Nature* **2009**, *461*, 629–632. [CrossRef] [PubMed]
33. Yu, K.; Lakhani, A.; Wu, M.C. Subwavelength Metal-Optic Semiconductor Nanopatch Lasers. *Opt. Express* **2010**, *18*, 8790. [CrossRef]
34. Lakhani, A.M.; Kim, M.; Lau, E.K.; Wu, M.C. Plasmonic Crystal Defect Nanolaser. *Opt. Express* **2011**, *19*, 18237. [CrossRef]
35. Ding, K.; Liu, Z.; Yin, L.; Wang, H.; Liu, R.; Hill, M.T.; Marell, M.J.H.; Van Veldhoven, P.J.; Nötzel, R.; Ning, C.Z. Electrical Injection, Continuous Wave Operation of Subwavelength-Metallic-Cavity Lasers at 260 K. *Appl. Phys. Lett.* **2011**, *98*, 231108. [CrossRef]
36. Sattar, Z.; Shore, K. Analysis of the Direct Modulation Response of Nanowire Lasers. *J. Lightwave Technol.* **2015**, *33*, 3028–3033. [CrossRef]
37. Sattar, Z.A.; Shore, K.A. External Optical Feedback Effects in Semiconductor Nanolasers. *IEEE J. Sel. Top. Quantum Electron.* **2015**, *21*, 500–505. [CrossRef]
38. Abdul Sattar, Z.; Ali Kamel, N.; Shore, K.A. Optical Injection Effects in Nanolasers. *IEEE J. Quantum Electron.* **2016**, *52*, 1200108. [CrossRef]
39. Han, H.; Shore, K.A. Dynamics and Stability of Mutually Coupled Nano-Lasers. *IEEE J. Quantum Electron.* **2016**, *52*, 2000306. [CrossRef]
40. Han, H.; Shore, K.A. Modulated Mutually Coupled Nano-Lasers. *IEEE J. Quantum Electron.* **2017**, *53*, 2000208. [CrossRef]
41. Romeira, B.; Fiore, A. Purcell Effect in the Stimulated and Spontaneous Emission Rates of Nanoscale Semiconductor Lasers. *IEEE J. Quantum Electron.* **2018**, *54*, 2000412. [CrossRef]
42. Wu, S.; Buckley, S.; Schaibley, J.R.; Feng, L.; Yan, J.; Mandrus, D.G.; Hatami, F.; Yao, W.; Vučković, J.; Majumdar, A.; et al. Monolayer Semiconductor Nanocavity Lasers with Ultralow Thresholds. *Nature* **2015**, *520*, 69–72. [CrossRef] [PubMed]
43. Elsonbaty, A.; Hegazy, S.F.; Obayya, S.S.A. Simultaneous Concealment of Time Delay Signature in Chaotic Nanolaser with Hybrid Feedback. *Opt. Lasers Eng.* **2018**, *107*, 342–351. [CrossRef]
44. Qu, Y.; Xiang, S.; Wang, Y.; Lin, L.; Wen, A.J.; Hao, Y. Concealment of Time Delay Signature of Chaotic Semiconductor Nanolasers with Double Chaotic Optical Injections. *IEEE J. Quantum Electron.* **2019**, *55*, 2000407. [CrossRef]
45. Abdul Sattar, Z.; Shore, K.A. Phase Conjugate Feedback Effects in Nano-Lasers. *IEEE J. Quantum Electron.* **2016**, *52*, 1100108. [CrossRef]

46. Jiang, P.; Zhou, P.; Li, N.; Mu, P.; Li, X. Optically Injected Nanolasers for Time-Delay Signature Suppression and Communications. *Opt. Express* **2020**, *28*, 26421. [CrossRef] [PubMed]
47. Zhang, X.; Guo, G.; Liu, X.; Hu, G.; Wang, K.; Mu, P. Dynamics and Concealment of Time-Delay Signature in Mutually Coupled Nano-Laser Chaotic Systems. *Photonics* **2023**, *10*, 1196. [CrossRef]